Chapter 3

Interaction among cracks in composite materials under the anti-plane shear loading

3.1 Introduction

3.1.1 Background and Motivation

The occurrence of cracks plays a pivotal role in dictating the strength and resilience of composite materials. The fracture resistance of any engineered structure is heavily influenced by the interfacial bonds that exist between disparate materials. Cracks may manifest during manufacturing or evolve due to repeated usage. The interface, being more prone to crack development, is often subjected to the effects of mismatched properties of the different materials involved. Consequently, examining

interfacial cracks within dissimilar orthotropic materials becomes a critical component in the fracture analysis of composite materials. This study provides valuable insights into such composites' structural integrity and durability. Anti-plane shear deformation is a class of deformations with which the solutions to solid mechanics problems can be examined more straightforwardly. The anti-plane shear crack problem provides a simplified yet practical approach to reviewing solutions to solid mechanics problems. In anti-plane shear deformations, the displacement is independent of the axial coordinates and perpendicular to the plane's direction. Anti-plane problems are simplified so that the governing equations consist of a single second-order linear partial differential equation. The mathematical treatment of these problems often involves using Fourier transforms and integral equations. For instance, the anti-plane crack problem can be reduced to a group of singular integral equations using the Fourier transform. Similarly, the problem of a finite crack in a strip is first reduced to two pairs of dual integral equations and then into Fredholm integral equations of the second kind. In conclusion, the study of anti-plane crack problems offers a simplified yet comprehensive approach to understanding the fracture behaviour of complex materials.

3.1.2 Literature survey

The presence of composite materials in engineering structures and their applications has encouraged many researchers to study the cracks in dissimilar isotropic materials [15, 74, 75, 76]. Williams [15] has worked on a problem with an application in fault lines dealing with the interface of two rock strata. Furthermore, in the anisotropic materials, the Investigations of cracks at the interface of the dissimilar medium can be found in many research articles [77, 78, 79, 80, 81, 82]. Clements [77], and Willis [83] have worked on the problems of a finite crack in dissimilar

anisotropic half-planes. They studied that the stresses are infinite near the end of the contact region. Ting [80] concluded that displacement oscillation is independent of the individual orientation of the two materials and is dependent on the material properties only. The anti-plane loading problem with a crack at the interface zone of the orthotropic strips was tackled in [84, 85] . Analyzing the co-existence of cracks in anisotropic materials is a complex phenomenon. Such crack interaction problems have been investigated in [86, 87, 88] and many more. The problem is converted into a set of integral equations, which are then solved numerically. Different Numerical methods are applied to calculate fracture mechanics parameters such as displacements, stresses and others. In the present problem, interaction effects such as amplification and shielding are also considered. The authors have found a closed-form solution in [89] for an orthotropic strip with a fracture susceptible to anti-plane shear force. Several research articles have [90, 91, 92] analyzed the s analyzed at the edge of a sharp line crack in an elastic plate due to anti-plane shear and uniform tension shear. In [93], the non-local elasticity field equations determine the stress in a plate with a Griffith crack subjected to the anti-plane shear. Knauss [94] has experimentally shown that cracks propagate in anti-plane shear without plasticity by opening semi-penny-shaped cracks at $\angle 45°$. In recent times, many research works have focused on anti-plane shear loading. In [95], the authors were devoted to analysing the stresses around rounded notches in orthotropic bodies subject to anti-plane shear loading by using the complex potential approach for anti-plane orthotropic elasticity with the conformal mapping technique. Physical quantities like SIF and COD were derived for a moving crack in semi-infinite half space in [96]. The authors employed the Fourier and inverse Fourier transformation techniques to convert the mixed boundary value problem. Also, as seen in [89], Li and Lee obtained the closed-form solution for an internal or edge crack under anti-plane shear. The results were shown graphically for normalised stress factors. Using the asymptotic

analysis, the asymptotic values of the stress and the displacement fields at crack tips for three collinear cracks were found in [97]. Das in [98] has investigated how three moving collinear Griffith cracks at an elastic layer's interface and a dissimilar half plane interact under anti-plane shear stress. Further, the author observed the shielding and amplification phenomena of the cracks, which depend on the crack spacing, their shared velocity of propagation, and the depth of the layer. In [99], the stress singularity at a crack tip with surface stresses along the crack surfaces is restricted to a problem of stress concentrations in the vicinity of mode III crack. Morse and Feshbach gave the Schmidt method [43] in the year 1954 and later was used by S. Itou [42] to determine coefficients in a series of a problem with a crack under static thermal loading conditions. The Schmidt method has been successfully applied to solve the present crack problem. The method has been used to solve the stress fields, displacement fields and SIFs in a non-complicated way. The motivation for this work comes from the interest in the interaction among offset cracks present in dissimilar orthotropic materials. Choi [100] studied the interaction among two offset parallel cracks embedded in Fiber-reinforced composite material under thermomechanical loadings. Under similar loading conditions, three cracks under static thermomechanical loadings were studied by Tanwar et al. [101]. In [102], the authors have investigated the behaviour of two symmetric parallel interfacial cracks under anti-plane shear stress loading. Das and Patra [103] studied dynamic SIFs in moving Griffith cracks in dissimilar orthotropic materials.

3.1.3 Chapter organisation

The chapter considers an anti-plane crack problem for dissimilar orthotropic materials. The governing equations and problem formulation for anti-plane shear have

been discussed in Section 3.2. The section contains boundary and continuity conditions for displacement fields and shear stress components. The Fourier integral transform and inverse Fourier technique have been employed to convert the mixed boundary value problem into dual integral equations. As done in the previous chapter, solution procedures to directly solve the integral equations without dealing with dual integrals are given in Section 3.3, which gives two equations containing two infinite series. The problem concerning shear stresses subjected to static loadings is investigated with the help of the Schmidt method, satisfying the given conditions. The difference in displacements is expanded to proceed further in the problem, which becomes zero outside the cracks. SIF expressions for mode III are obtained in Section 3.4. The graphical representations of normalised SIFs at all crack tips vs. the ratio of crack lengths are done for different values of the width of the strip. Numerical computations have been done to show the interactions among the cracks for different combinations of materials, viz. aluminium, graphite epoxy and epoxy given in Section 3.5. A detailed analysis of obtained numerical results has been done in this section. At the end of the chapter, the Conclusion Section 3.6 is added to give the overall remarks about the work of the current chapter.

3.2 Formulation of problem

Consider a problem comprising of an infinitely long strip of width h bonded between two dissimilar orthotropic half-planes, containing a central crack at the interface $y = 0$ and two symmetrical cracks at the interface $y = h$ of the composite materials. The cracks are such that they align with the x axis. The Cartesian coordinate system (x, y) is considered here. The cracks occupy the coordinates $-a \leq x \leq a$ at $y = 0$,

$-c \leq x \leq -b$ and $b \leq x \leq c$ at $y = h$ as depicted in Figure 3.1. It is assumed that the cracks are under the influence of time-independent anti-plane shear traction.

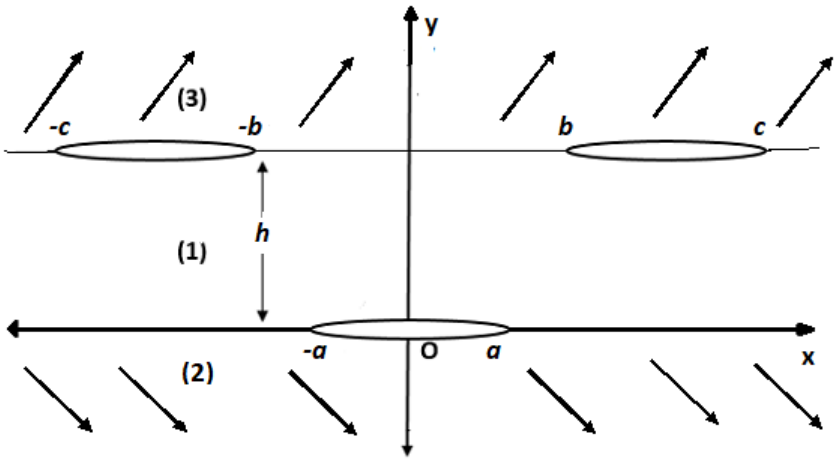

FIGURE 3.1: Geometry of the problem with three cracks at the interfaces of orthotropic materials under anti-plane shear traction.

3.2.1 Governing equations

In the anti-plane and in the absence of body forces, the governing linear homogeneous partial differential equation is given in this section. The equation of motion for the concerned medium is given by [104]

$$C_{55}^{(i)}\ \omega_{,xx}^{(i)} + C_{44}^{(i)}\ \omega_{,yy}^{(i)} = 0, \tag{3.1}$$

where the superscript i is used to depict the three dissimilar orthotropic materials, namely the bonded strip 1, lower half plane 2 and upper half plane 3 in $(0 < y < h,\ -\infty < y < 0,\ h < y < \infty)$, respectively. Here, $\omega(x, y)$ is the out-of-plane displacement field and C_{44} , C_{55} are parameters for the corresponding orthotropic materials.

Applying equation (1.28a) in equation (3.1), we obtain

$$\overline{\omega}^{(i)}_{,yy} - s^2\ k^{(i)2}\ \overline{\omega} = 0, \tag{3.2}$$

where $k^{(i)} = \sqrt{C^{(i)}_{55}/C^{(i)}_{44}}$ and s is the transformation variable. Further, by solving equation (3.2) and making use of the regularity condition for the displacement field, we obtain three expressions for displacements in three mediums as

$$\overline{\omega}^{(1)}(s,y) = (A^{(1)}(s)\ e^{sk^{(1)}y} + B^{(1)}(s)\ e^{-sk^{(1)}y})\ ,\quad 0 \le y \le h, \tag{3.3a}$$

$$\overline{\omega}^{(2)}(s,y) = A^{(2)}(s)\ e^{sk^{(2)}y}\ ,\quad y \le 0, \tag{3.3b}$$

$$\overline{\omega}^{(3)}(s,y) = A^{(3)}(s)\ e^{-sk^{(3)}y}\ ,\quad y \ge h. \tag{3.3c}$$

The unknowns $A^{(i)}$'s and $B^{(1)}$'s are functions of transformation variable s. Let $\tau_{zk},\ k = x, y$ be anti-plane shear stress component and it is given by [104]

$$\tau_{xz} = C_{55}\ \omega_{,x}\ ,\ \tau_{yz} = C_{44}\ \omega_{,y}. \tag{3.4}$$

Let us define the Domain τ_1 and τ_2 to depict the positioning of the cracks where τ_1 represents $\{(x,y)|\ x \in (-c,-b) \cup (b,c)\ \&\ y = h\}$ and τ_2 represents $\{(x,y)|\ x \in (-a,a)\ \&\ y = 0\}$.

3.2.2 Boundary and continuity conditions

Owning to the geometry of the problem and the loading conditions, the continuity and boundary conditions along the interfaces for the considered problem are given by

$$\tau^{(1)}_{yz}(x,h) = \tau^{(3)}_{yz}(x,h) = -p_1(x),\quad x \in \tau_1, \tag{3.5a}$$

$$\tau_{yz}^{(1)}(x,0) = \tau_{yz}^{(2)}(x,0) = -p_2(x), \quad x \in \tau_2, \tag{3.5b}$$

$$\tau_{yz}^{(1)}(x,h) = \tau_{yz}^{(3)}(x,h), \quad x \in \mathbb{R}, \tag{3.5c}$$

$$\tau_{yz}^{(1)}(x,0) = \tau_{yz}^{(2)}(x,0), \quad x \in \mathbb{R}, \tag{3.5d}$$

$$\omega^{(1)}(x,h) = \omega^{(3)}(x,h), \quad x \in \tau_1^c, \tag{3.5e}$$

$$\omega^{(1)}(x,0) = \omega^{(2)}(x,0), \quad x \in \tau_2^c, \tag{3.5f}$$

$$\omega^{(i)}(x,y) = 0, \ i = 1,2,3, \quad (x^2+y^2)^{1/2} \to \infty, \tag{3.5g}$$

where p_1 and p_2 are mechanical loadings. They are considered positive values for our problem. Equation (3.5g) is the regularity condition. From the definition in equation (3.4), we obtain the expressions for shear stresses as

$$\overline{\tau}_{yz}^{(1)}(s,y) = \ s\mu_1(A^{(1)}\ e^{sk^{(1)}y} - B^{(1)}\ e^{-sk^{(1)}y}), \tag{3.6a}$$

$$\overline{\tau}_{yz}^{(2)}(s,y) = \ s\mu_2 A^{(2)}\ e^{sk^{(2)}y}\ , \tag{3.6b}$$

$$\overline{\tau}_{yz}^{(3)}(s,y) = \ s\mu_3 A^{(3)}\ e^{-sk^{(3)}y}\ , \tag{3.6c}$$

where $\mu_i = \sqrt{C_{44}^{(i)}\ C_{55}^{(i)}}$.

3.3 Solution of the problem

Applying the conditions established in the previous section, we can obtain the set of integral equations with infinite integrals. To proceed further, making use of the displacement continuity condition given by equations (3.5e), (3.5f), we introduce auxiliary functions, which are the jumps in the displacements across the interfaces

as

$$f_1(x) = \omega^{(3)}(x,h) - \omega^{(1)}(x,h), \tag{3.7a}$$

$$f_2(x) = \omega^{(1)}(x,0) - \omega^{(2)}(x,0). \tag{3.7b}$$

Mathematical calculations on applying boundary conditions (3.5e), (3.5f) in equations (3.7) and by substituting the equations in (3.3) into the above equations and then applying the boundary conditions in (3.5a), (3.5b), give rise to

$$\int_0^\infty \overline{f}_1(s)\ \cos(sx)\ ds = 0, \quad x \in \tau_1^c, \tag{3.8a}$$

$$\int_0^\infty \overline{f}_2(s)\ \cos(sx)\ ds = 0, \quad x \in \tau_2^c, \tag{3.8b}$$

$$\sqrt{\frac{2}{\pi}} \int_0^\infty \Big(\overline{f_1}(s)\ g_1(s)\Big) - \overline{f_2}(s)\ g_2(s)\Big) s\ \cos(sx)ds = -p_1(x), \quad x \in \tau_1, \tag{3.8c}$$

$$\sqrt{\frac{2}{\pi}} \int_0^\infty \Big(\overline{f_1}(s)\ g_3(s) - \overline{f_2}(s)\ g_4(s)\Big) s\ \cos(sx)ds = -p_2(x), \quad x \in \tau_2, \tag{3.8d}$$

where $\lim\limits_{s\to\infty} g_1(s) = \beta_1$ and $\lim\limits_{s\to\infty} g_2(s) = \beta_2$. Similarly, $\lim\limits_{s\to\infty} g_3(s) = \beta_3$ and $\lim\limits_{s\to\infty} g_4(s) = \beta_4$. In the above equations, $g_i,\ \beta_i, i = 1(1)4$ are known functions. For the single identical plane problem, $\beta_1 = -C_{44}^{(1)}/2$, which coincides with the values in [102]. Further, the above equations can be rewritten as

$$\begin{aligned}\int_0^\infty \Bigg(\overline{f_1}(s)\ \Bigg(&\frac{(1+\frac{\mu_1}{\mu_2}) + (1-\frac{\mu_1}{\mu_2})e^{-2sk^{(1)}h}}{(1+\frac{\mu_1}{\mu_3})(1+\frac{\mu_1}{\mu_2}) - (1-\frac{\mu_1}{\mu_3})(1-\frac{\mu_1}{\mu_2})e^{-2sk^{(1)}h}} - \frac{\mu_3}{\mu_3+\mu_1}\Bigg) \\ - \overline{f_2}(s)\ e^{-sk^{(1)}h}\ \Bigg(&\frac{(1+\frac{\mu_1}{\mu_3}) + (1-\frac{\mu_1}{\mu_3})}{(1+\frac{\mu_1}{\mu_3})(1+\frac{\mu_1}{\mu_2}) - (1-\frac{\mu_1}{\mu_3})(1-\frac{\mu_1}{\mu_2})e^{-2sk^{(1)}h}}\Bigg)\Bigg) s\ \cos(sx)\ ds \\ &= -\sqrt{\frac{\pi}{2}}\frac{p_1(x)}{\mu_1},\end{aligned} \tag{3.9a}$$

$$\int_0^\infty \left(\overline{f_1}(s)\ e^{-sk^{(1)}h} \left(\frac{(1+\frac{\mu_1}{\mu_2})+(1-\frac{\mu_1}{\mu_2})}{(1+\frac{\mu_1}{\mu_3})(1+\frac{\mu_1}{\mu_2})-(1-\frac{\mu_1}{\mu_3})(1-\frac{\mu_1}{\mu_2})e^{-2sk^{(1)}h}} \right) \right.$$
$$\left. - \overline{f_2}(s) \left(\frac{(1+\frac{\mu_1}{\mu_3})+(1-\frac{\mu_1}{\mu_3})e^{-2sk^{(1)}h}}{(1+\frac{\mu_1}{\mu_3})(1+\frac{\mu_1}{\mu_2})-(1-\frac{\mu_1}{\mu_3})(1-\frac{\mu_1}{\mu_2})e^{-2sk^{(1)}h}} - \frac{\mu_2}{\mu_2+\mu_1} \right) \right) s\ \cos(sx)\ ds$$
$$= -\sqrt{\frac{\pi}{2}} \frac{p_2(x)}{\mu_1}. \tag{3.9b}$$

Now, the aim is to solve the dual integral equations given in equations (3.8a)-(3.8d). To solve the said equations, the difference in displacement at $y = h$, $y = 0$ can be represented as the series of Jacobi polynomial [40] as

$$f_1(x) = \sum_{n=1}^{\infty} b_n\ P_{n-1}^{(1/2,1/2)} \left(\frac{x - \frac{c+b}{2}}{\frac{c-b}{2}} \right) \left(1 - \frac{\left(x - \frac{c+b}{2}\right)^2}{\left(\frac{c-b}{2}\right)^2} \right)^{1/2}, \quad x \in \tau_1, \tag{3.10}$$

$$f_2(x) = \sum_{n=1}^{\infty} c_n\ P_{2n-2}^{(1/2,1/2)} \left(\frac{x}{a}\right) \left(1 - \frac{x^2}{a^2} \right)^{1/2}, \quad x \in \tau_2, \tag{3.11}$$

where b_n and c_n are unknown coefficients to be determined, $P_n(x)$ is the Jacobi polynomial. From equations (3.10) and (3.11), we obtain [105]

$$\overline{f}_1(s) = \sum_{n=1}^{\infty} b_n\ G_1(s)\ B_n(s)\ \frac{1}{s}\ J_n\big(s\ \frac{(c-b)}{2}\big), \tag{3.12}$$

$$\overline{f}_2(s) = \sum_{n=1}^{\infty} (-1)^{n-1} c_n\ G_2(s)\ \ \frac{1}{s}\ J_{2n-1}(s\ a), \tag{3.13}$$

where $J_n(s)$ is Bessel's function and $G(s)$ are Gamma functions. Values of the known functions are all given in the Appendix A. Integrating both the equations from $[0, x]$

and $[b, x]$ respectively, we get

$$\int_0^\infty \sum_{n=1}^{\infty}(-1)^{n-1}\ b_n\ G_1\ B_n(s)\frac{1}{s}J_n(s\ (c-b)/2)\ g_1(s)\ (\sin(sx)-\sin(sb))\ ds$$
$$+\int_0^\infty \sum_{n=1}^{\infty} c_n\ G_2\ \frac{1}{s}\ J_{2n-1}(sa)\ \ g_2(s)\ (\sin(sx)-\sin(sb))\ ds = \sqrt{\frac{\pi}{2}}\ \frac{p_1(x)}{\mu_1}\ (x-b), \tag{3.14}$$

$$\int_0^\infty \sum_{n=1}^{\infty} c_n\ G_2\ B_n(s)\ \frac{1}{s}\ J_{2n-1}(s\ (c-b)/2)\ g_4(s)\ (\sin(sx)-\sin(sa))\ ds$$
$$+\int_0^\infty \sum_{n=1}^{\infty}(-1)^{n-1}\ b_n\ G_1\ \frac{1}{s}J_{2n-1}(sa)\ g_3(s)\sin(sx)\ ds = \sqrt{\frac{\pi}{2}}\ \frac{p_2(x)\ x}{\mu_1}. \tag{3.15}$$

Substituting the equations (3.14)-(3.15) into the equations (3.6), we get

$$\overline{\tau}_{yz}^{(1)}(s,h) = \sum_{n=1}^{\infty} b_n\ G_1\ J_n(s(c-b)/2)\ g_1(s)$$
$$+\sum_{n=1}^{\infty} c_n\ G_2(-1)^{n-1}\ J_{2n-1}(s\ a)\ g_2(s)\ \cos(s\ (c+b)/2)\ , \tag{3.16}$$

$$\overline{\tau}_{yz}^{(1)}(s,0) = \sum_{n=1}^{\infty} b_n\ G_1 B_n(s)\ J_n(s(c-b)/2)\ g_3(s)$$
$$+\sum_{n=1}^{\infty} c_n\ G_2(-1)^{n-1}\ J_{2n-1}(s\ a)\ g_4(s)\ . \tag{3.17}$$

The above equations in (3.14) and (3.15) can be rewritten as a system of algebraic equations which are solved for the unknowns using the Schmidt method 1.7.2.

3.4 Stress intensity factors

Now, consider the singular parts (SPs) of the stress fields given in equations (3.16) and (3.17) and we obtain the following expressions as

$$\begin{aligned}\tau_{yz}{}^{(1)}(x,h)\big]_{SP} = \\ -\sqrt{\frac{2}{\pi}}\sum_{n=1}^{\infty} b_n G_n (-1)^{n-1}\beta_1 \frac{\left(\frac{c-b}{2}\right)^{2n-1}\sin\left((2n-1)\frac{\pi}{2}\right)}{\sqrt{\left(\frac{c+b}{2}-x\right)^2-\left(\frac{c-b}{2}\right)^2}\left[\frac{(c+b)}{2}-x+\sqrt{\left(\frac{c+b}{2}-x\right)^2-\left(\frac{c-b}{2}\right)^2}\right]^{2n-1}} \\ -\frac{\left(\frac{c-b}{2}\right)^{2n-1}\sin\left((2n-1)\frac{\pi}{2}\right)}{\sqrt{\left(\frac{c+b}{2}+x\right)^2-\left(\frac{c-b}{2}\right)^2}\left[\frac{(c+b)}{2}+x+\sqrt{\left(\frac{c+b}{2}+x\right)^2-\left(\frac{c-b}{2}\right)^2}\right]^{2n-1}},\end{aligned} \tag{3.18}$$

$$\tau_{yz}^{(1)}(x,0)\big]_{SP} = \sqrt{\frac{2}{\pi}}\sum_{n=1}^{\infty} c_n G_n (-1)^{n-1}\beta_4\left(-\frac{a^{2n-1}\sin\left((2n-1)\frac{\pi}{2}\right)}{\sqrt{x^2-a^2}\left[x+\sqrt{x^2-a^2}\right]^{2n-1}}\right). \tag{3.19}$$

The results for the Stress intensity factor at the tips of the cracks can be obtained as [102]

$$K_a = \lim_{x\to a+}\sqrt{2\,\pi\,(x-a)}\,\tau_{yz}^{(2)}(x,0) = -4\,\sqrt{\pi}\,\beta_4\sum_{n=1}^{\infty} c_n\,\frac{1}{\sqrt{2a}}\,\frac{\Gamma(2n-1/2)}{(2n-2)!}, \tag{3.20}$$

$$K_b = \lim_{x\to b-}\sqrt{2\,\pi\,(b-x)}\,\tau_{yz}^{(3)}(x,h) = -4\,\sqrt{\pi}\,\beta_1\sum_{n=1}^{\infty} b_n\,\frac{1}{\sqrt{c-b}}\,\frac{\Gamma(n+3/2)}{n!}, \tag{3.21}$$

$$K_c = \lim_{x\to c+}\sqrt{2\,\pi\,(x-c)}\,\tau_{yz}^{(3)}(x,h) = 4\,\sqrt{\pi}\,\beta_1\sum_{n=1}^{\infty}(-1)^{n-1}b_n\,\frac{1}{\sqrt{c-b}}\,\frac{\Gamma(n+3/2)}{n!}. \tag{3.22}$$

The normalised SIFs at the crack tip $x = a$ is defined by $K_a^* = K_a/K_o$ and for the crack tip $x = b$ and $x = c$ is defined by $K_b^* = K_b/K_o$, $K_c^* = K_c/K_o$ where $K_o = p_2\sqrt{\pi a}$ for crack tip a and $K_o = p_1\sqrt{\pi(c-b)/2}$ for crack tips b and c.

3.5 Numerical results and discussion

	aluminium	epoxy	graphite epoxy
$C_{44}(\times 10^{10} N/m^2)$	2.65	0.176	0.361
$C_{55}(\times 10^{10} N/m^2)$	2.65	0.176	0.565

TABLE 3.1: Table of values of material parameters used in the problem.

To show the dependency of SIFs on the crack length and width of the strip, three dissimilar orthotropic materials, aluminium, epoxy, and graphite epoxy, have been considered, and their respective values [106] are given in Table 3.1. To compute the integrals presented in equations (3.14) and (3.15), we employ an adaptive Gaussian quadrature technique. We then proceed to graphically represent the normalised SIFs using the factor $K_o = \tau_o\sqrt{\pi l}$, where τ_o is the constant load p_1 or p_2 at a given point, and l is half the crack length. The loads p_1 and p_2 in equations (3.5a) and (3.5b) are considered as identical positive constants. We plot the graphs for the normalised SIFs, $K_a^* = K_a/K_o$, $K_b^* = K_b/K_o$, and $K_c^* = K_c/K_o$ at the three crack tips against the ratio of crack lengths d/a, where $d = (c-b)/2$. We consider varying values of the width of the horizontal strip h for all cases. The authors have observed variations in SIFs for the cracks at the interfaces of different materials. In Case 1, we consider all materials for the three layers, with aluminium as medium 1, graphite as medium 2, and epoxy as medium 3. Figure 3.2, 3.3, and 3.4 represent the plots of the normalised SIFs at all crack tips for this case. In Case 2, material 3 is replaced by material 2; hence, materials 2 and 3 are identical graphite epoxy materials. Figure 3.5, 3.6, and 3.7 represent the plots of normalised SIFs at all crack tips for this case. In Case 3, material 2 is replaced by epoxy. Hence, materials 2 and 3 are identical epoxy materials. Figure 3.8, 3.9, and 3.10 represent the plots of normalised SIFs at all crack tips for this case. We use the Schmidt method to solve the mathematical model in question during computations. This method has successfully computed the stress fields, displacement fields, and SIFs in a straightforward manner.

From the numerical computations and graphical results, the following can be concluded by the authors,

- In all the cases, it has been considered that the values of SIFs for $h = 0$ are dominant for all three crack tips irrespective of the material choices, and consequently, as the width of the strips consisting of the offset cracks increases, the curves for values of SIFs lie at the lower ranges. This is due to the closeness of cracks and high Interaction among those as the value of h is less. It can be noted pictorially that as h increases, SIFs decrease. This variation is shown graphically for values $h = 0$, $h = 1$ and $h = 2$. The values for h can be taken higher, but the authors have chosen the values to reflect the effect of the strip width on the SIFs at the three crack tips.

- In Case 1, for the considered offset finite cracks in an infinite orthotropic plane, the SIFs attain a peak value at $d/a = 0.36$ for K_b^* and at $d/a = 0.165$ for K_a^* and K_c^*. For all the material combinations in Cases 1, 2 and 3 that are taken into account, K_b^* is the one that attains maximum value, and as the ratio d/a increases, the values tend to decrease. The maximum SIF attained at crack tip b is 2.276 at the point $d/a = 0.36$.

- In all the cases, it can be noted that when the interfacial cracks are close, the curves display complicated behaviour, mainly when the ratio d/a is less than 0.83. After a certain point, the curves show stable behaviour. It is because of the interaction among cracks when the ratio is less, and both the offset cracks influence the stress fields at the tips of each crack to a much greater extent. When the cracks are away from each other, such influence is less, and it can be seen as the curves' fluctuations become more stable for a higher ratio of crack lengths. The mutual interactions among the cracks are seen in the graphs, and as the cracks move away from each other, the fluctuations become less.

- As the crack length ratio, i.e., d/a, is increasing, there is a decreasing effect on SIFs at the tips of the cracks. This can be seen in all the cases where there is a sudden drop in the values for SIFs after attaining the peak values, but after that, the SIFs decrease gradually.

- The curves show slightly similar behaviour for the values of K_a^*, K_b^*, K_c^*. But the values of $K_c^* << K_a^* << K_b^*$ vary considerably with the change in ratio d/a and values of h.

3.6 Conclusion

In the given chapter, an anti-plane stress problem involving three cracks within dissimilar orthotropic materials is meticulously examined. The mixed boundary value problem is converted into a set of dual integral equations, which are then solved using the Schmidt method, a well-established numerical technique for solving integral equations. The study considers three distinct combinations of materials, namely Aluminium, Graphite epoxy, and Epoxy. These materials are commonly used in various engineering applications, and understanding their fracture mechanics is crucial for improving their performance and durability. The authors have successfully determined the variations in SIF of mode III for the cracks located in these dissimilar composite materials. The SIF is a critical parameter in fracture mechanics, as it quantifies the stress field near the crack tip and predicts the potential for crack propagation. To facilitate a comprehensive understanding of the interactions of the cracks within the considered model, the authors have plotted graphs depicting the normalised SIFs at all crack tips against the ratio of crack lengths. These graphs are presented for different values of the width of the horizontal strip, denoted by h. This detailed analysis provides valuable insights into the behaviour of cracks in

dissimilar orthotropic materials and contributes significantly to the field of fracture mechanics. It also aids in designing and developing more robust and durable composite materials for various engineering applications. The finite crack length can be extended to the study of a semi-infinite crack model or edge crack model, which are a form of very commonly occurring fractures at the interface of the orthotropic medium. The problem has been tackled in the next chapter of the thesis.

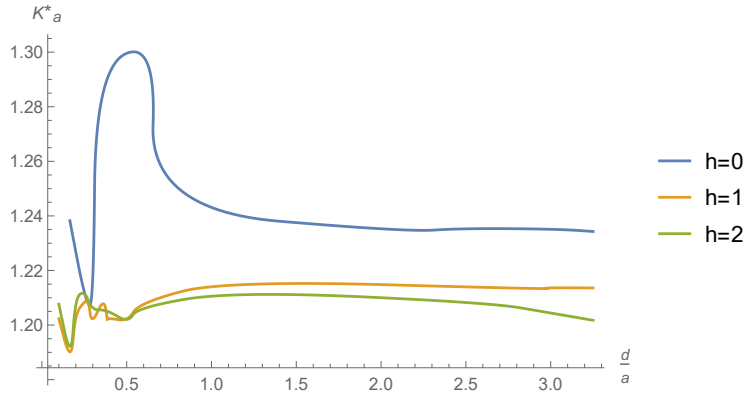

FIGURE 3.2: The plots of the normalised SIFs K_a^* vs. crack length ratio d/a for $h = 0,\ h = 1,\ h = 2$ for aluminium, graphite epoxy, epoxy as media 1, 2 and 3, respectively for Case 1.

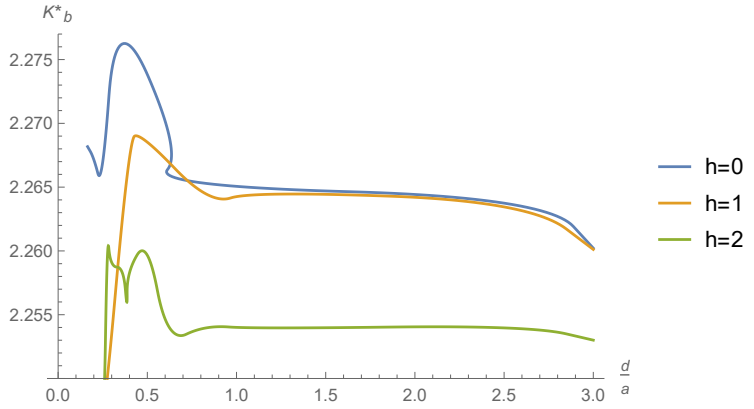

FIGURE 3.3: The plots of the normalised SIFs K_b^* vs. crack length ratio d/a for $h = 0,\ h = 1,\ h = 2$ for aluminium, graphite epoxy, epoxy as media 1, 2 and 3, respectively for Case 1.

****

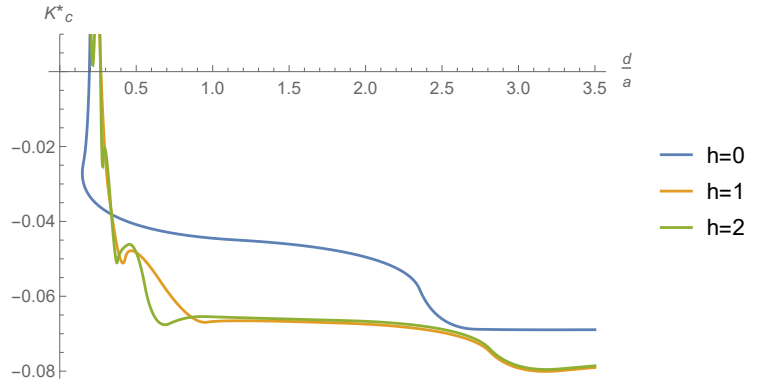

FIGURE 3.4: The plots of the normalised SIFs K_c^* vs. crack length ratio d/a for $h = 0,\ h = 1,\ h = 2$ for aluminium, graphite epoxy, epoxy as media 1, 2 and 3, respectively for Case 1.

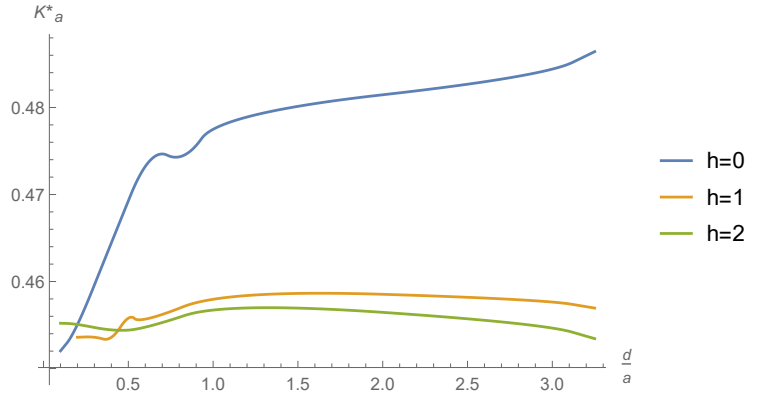

FIGURE 3.5: The plots of the normalised SIFs K_a^* vs. crack length ratio d/a for $h = 0,\ h = 1,\ h = 2$ for aluminium, graphite epoxy, graphite epoxy as media 1, 2 and 3, respectively for Case 2.

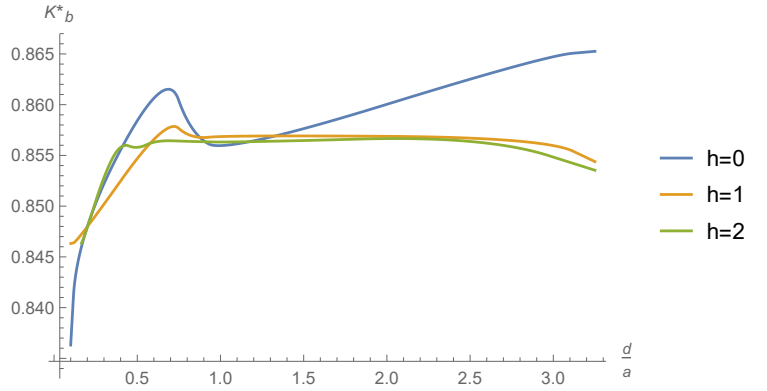

FIGURE 3.6: The plots of the normalised SIFs K_b^* vs. crack length ratio d/a for $h = 0,\ h = 1,\ h = 2$ for aluminium, graphite epoxy, graphite epoxy as media 1, 2 and 3, respectively for Case 2.

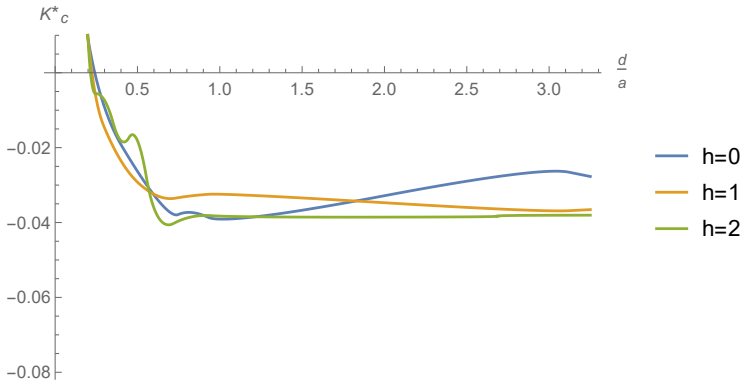

FIGURE 3.7: The plots of the normalised SIFs K_c^* vs. crack length ratio d/a for $h = 0,\ h = 1,\ h = 2$ for aluminium, graphite epoxy, graphite epoxy as media 1, 2 and 3, respectively for Case 2.

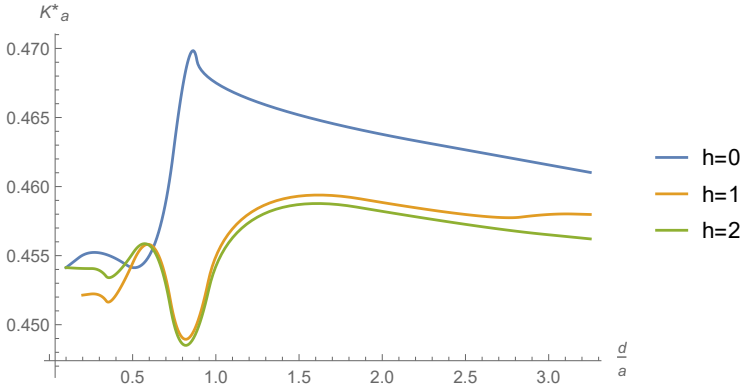

FIGURE 3.8: The plots of the normalised SIFs K_a^* vs. crack length ratio d/a for $h = 0, h = 1, h = 2$ for aluminium, epoxy, epoxy as media 1, 2 and 3, respectively for Case 3.

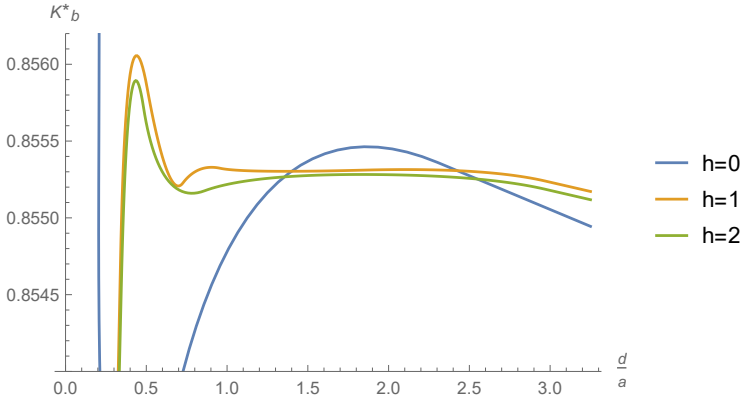

FIGURE 3.9: The plots of the normalised SIFs K_b^* vs. crack length ratio d/a for $h = 0, h = 1, h = 2$ for aluminium, epoxy, epoxy as media 1, 2 and 3, respectively for Case 3.

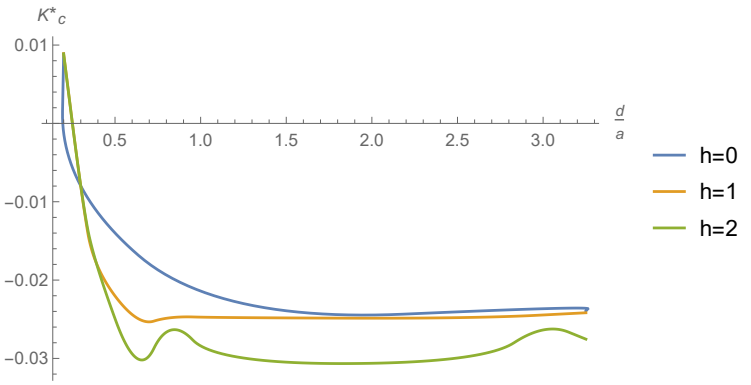

FIGURE 3.10: The plots of the normalised SIFs K_c^* vs. crack length ratio d/a for $h = 0, h = 1, h = 2$ for aluminium, epoxy, epoxy as media 1, 2 and 3, respectively for Case 3.